X-ray scattering study of actin polymerization nuclei assembled by tandem W domains

Grzegorz Rebowski*†, Malgorzata Boczkowska*†, David B. Hayes‡, Liang Guo§, Thomas C. Irving§, and Roberto Dominguez†¶

†Department of Physiology, School of Medicine, University of Pennsylvania, Philadelphia, PA 19104; ‡Boston Biomedical Research Institute, Watertown, MA 02472; and §BioCAT, Department of Biological, Chemical, and Physical Sciences, Illinois Institute of Technology, Chicago, IL 60616

Edited by Clara Franzini-Armstrong, University of Pennsylvania School of Medicine, Philadelphia, PA, and approved May 28, 2008 (received for review February 20, 2008)

The initiation of actin polymerization in cells requires actin filament nucleators. With the exception of formins, known filament nucleators use the Wiskott–Aldrich syndrome protein (WASP) homology 2 (WH2 or W) domain for interaction with actin. A common architecture, found in Spire, Cobl, VopL, and VopF, consists of tandem W domains that tie together three to four actin monomers to form a polymerization nucleus. Uncontrollable polymerization has prevented the structural investigation of such nuclei. We have engineered stable nuclei consisting of an actin dimer and a trimer stabilized by tandem W domain hybrid constructs and studied their structures in solution by x-ray scattering. We show that Spire-like tandem W domains stabilize a polymerization nucleus by lining up actin subunits along the long-pitch helix of the actin filament. Intersubunit contacts in the polymerization nucleus, thought to involve the DNase I-binding loop of actin, coexist with the binding of the W domain in the cleft between actin subdomains 1 and 3. The successful stabilization of filament-like multiactin assemblies opens the way to the crystallographic investigation of intersubunit contacts in the actin filament.

actin nucleation | cytoskeleton dynamics | WH2 domain

The spontaneous polymerization of actin filaments is inhibited in cells by actin monomer-binding proteins such as profilin and thymosin-β4 (Tβ4). Cells use filament nucleators to stabilize actin polymerization nuclei, whose formation is rate-limiting during actin assembly (1). In addition to Arp2/3 complex and formins (2), a number of filament nucleators have been recently discovered: Spire (3), Cobl (4), VopL (5), VopF (6), and Lmod (7). With the exception of formins, all filament nucleators use the W domain for interaction with actin.

The W domain is a short actin-binding motif of 17–27 aa (8). The N-terminal portion of the W domain forms a helix that binds in the cleft between actin subdomains 1 and 3 at the barbed end of the actin monomer (9). After this helix, the W domain presents an extended region that climbs toward the pointed end of the actin monomer. This portion of the W domain has variable length and sequence but comprises the conserved four-aa motif LKKT(V). Tβ4, a member of the W domain family, contains an additional helix at the C terminus, which binds atop actin subdomains 2 and 4 and caps the pointed end (10).

The W domain frequently occurs in tandem repeats. Tandem W domains constitute a common architecture among actin filament nucleators, such as Spire, Cobl, VopL, and VopF (Fig. 1*A*). The actin monomers bound to the individual W domains of these proteins are thought to come together to form a filament-like nucleus for polymer assembly. This proposal, however, has not been directly demonstrated. An apparent contradiction is that the cleft between actin subdomains 1 and 3, where the N-terminal helix of the W domain binds, is also thought to participate in intersubunit contacts in the actin filament (11–13). Therefore, it remains to be demonstrated whether and how tandem W domains stabilize actin monomers into a filament-like structure. To answer this question, we made hybrid constructs consisting of two or three W domains followed by the pointed end capping C-terminal helix of Tβ4. These constructs form stable complexes with two or three actin subunits. The conformation of the complexes studied in solution by using small-angle x-ray scattering (SAXS) appears indistinguishable from that of the long-pitch helix of the actin filament (11).

Results

Engineering Stable Actin Polymerization Nuclei. Actin polymerization nuclei evolve rapidly into filaments, making their structural investigation particularly challenging. In an attempt to capture the primary nucleus stabilized by tandem W domains such as those found in filament nucleators, we engineered hybrid constructs that form stable complexes with actin. Two constructs were made, containing either two or three W domains and referred to as 2W and 3W (Fig. 1 *A* and *B*). Both constructs are based on the pair of W domains found in N-WASP, followed by the pointed end-capping region of Tβ4. Thus, construct 2W consists of mouse N-WASP residues Ala-397–Lys-444 and Tβ4 residues Lys-20–Ser-44. The two proteins were fused within the LKKT(V) motifs of the second W domain of N-WASP and that of Tβ4 (Fig. 1*A*). This site was chosen because of its conserved sequence and because individually determined structures of actin complexes with W domains (9) and Tβ4 (10) overlie well in this region [supporting information (SI) Fig. S1]. From the structures of W domains bound to actin we determined that Pro-398 binds within disulfide bond distance to actin Cys-374. Therefore, we introduced a Cys residue at this position to cross-link the first W domain of construct 2W to actin Cys-374, which we anticipated would cap the barbed end of the polymerization nucleus (Fig. 1 *A* and *B*). To ensure that no other cross-linking site was present, we also replaced the endogenous Cys-427 by Ala, a common amino acid at this position. Construct 3W was generated from 2W with duplication of the second W domain of N-WASP (residues Glu-419–Lys-444), inserted after N-WASP residue Val-446 and followed by Tβ4 residues Lys-20–Ser-44 (Fig. 1*A*).

Constructs 2W and 3W were mixed with a slight molar excess of actin, compared with the number of W domains present in each construct. Both constructs appeared to bind actin cooperatively. Thus, analysis by native gel electrophoresis showed that independent of mixing ratio construct 2W always bound two actin molecules (Fig. 1*C*). Construct 3W bound two or three

Author contributions: R.D. designed research; G.R., M.B., and D.B.H. performed research; L.G. and T.C.I. contributed new reagents/analytic tools; G.R. and M.B. analyzed data; and R.D. wrote the paper.

The authors declare no conflict of interest.

This article is a PNAS Direct Submission.

*G.R. and M.B. contributed equally to this work.

¶To whom correspondence should be addressed: E-mail: droberto@mail.med.upenn.edu.

This article contains supporting information online at www.pnas.org/cgi/content/full/0801650105/DCSupplemental.

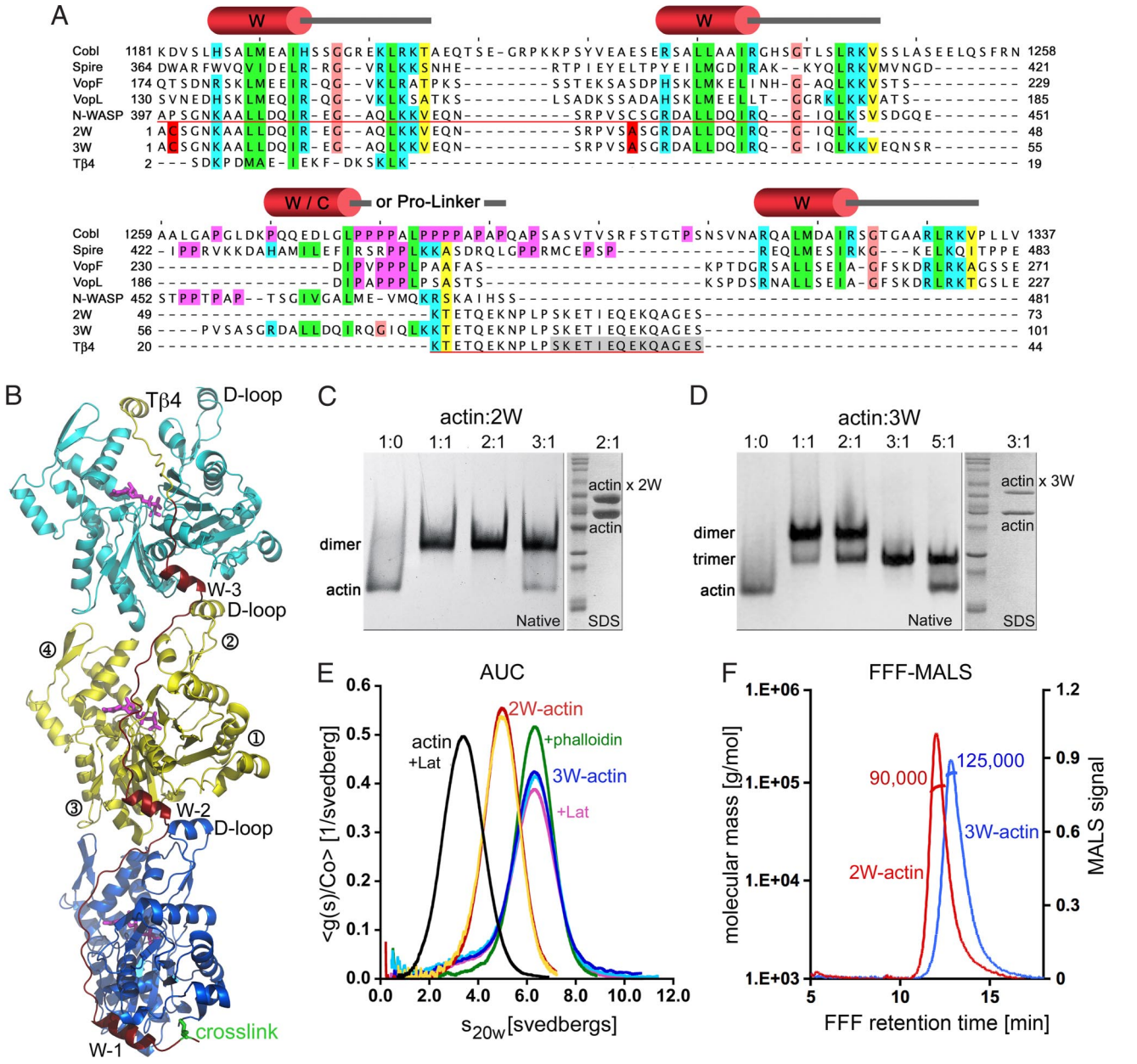

Fig. 1. Design and characterization of the complexes of 2W-actin and 3W-actin. (*A*) Alignment of W-based filament nucleators and hybrid constructs used in this work. Accession numbers: Cobl (mouse, CAI36023); Spire (*Drosophila melanogaster*, Q9U4F1); VopF (*Vibrio cholerae*, AAZ32252); VopL (*Vibrio parahaemolyticus*, NP_800881); N-WASP (mouse, CAC69994); and Tβ4 (mouse, NP_067253). Underlined red are the fragments of N-WASP and Tβ4 fused to generate construct 2W. Residues Pro-398 and Cys-427 were mutated to Cys and Ala, respectively (red background). Construct 3W was generated from 2W with duplication of N-WASP residues Glu-419–Lys-444. Conserved residues are colored according to their chemical characteristics (green, hydrophobic; blue, basic; magenta, prolines; brown, glycines; yellow, small conserved amino acid). The N-terminal portion of the W domain forms a helix (diagram) followed by an extended region that contains the conserved motif LKKT(V). (*B*) Model of 3W-actin obtained by superimposing the structure of W-actin (9) onto three consecutive subunits of the long-pitch helix of the actin filament (11). The C-terminal portion of Tβ4 was modeled according to the structure of its complex with actin (10). Subdomains 1–4 of actin are labeled for the middle actin subunit. (*C* and *D*) In native gels actin runs faster than 3W-actin, which runs faster than 2W-actin. 2W binds two actins independent of mixing ratio. 3W first binds two and then three actins. Nonreducing SDS gels show free actin and actin cross-linked to 2W and 3W. (*E*) Actin with latrunculin (Lat) and the complexes of 2W-actin and 3W-actin (+/− Lat or phalloidin) form single species, which were well separated by AUC, with S values of 3.47, 5.02, and 6.43. (*F*) Determination of molecular masses by FFF-MALS: 2W-actin, 90,000 Da (expected 92,038 Da); and 3W-actin, 125,000 Da (expected 137,161 Da).

actin molecules when actin was present in <3-fold molar excess (Fig. 1*D*). In the presence of 3-fold or higher molar excess of actin, all three actin-binding sites of 3W were saturated. Analysis by nonreducing denaturing gel electrophoresis showed that one of the actin molecules was covalently cross-linked to constructs 2W and 3W (Fig. 1 *C* and *D*).

Excess actin was separated from the complexes of 2W-actin and 3W-actin by size exclusion chromatography. The stability and homogeneity of the complexes were investigated by analytical ultracentrifugation. Both complexes formed single species in high-salt polymerization buffer, which were clearly distinguishable from each other and from actin (Fig. 1*E*). The sedimentation coefficient of actin with bound latrunculin, a marine toxin that prevents actin polymerization (14), was 3.47S, compared with 5.02S for 2W-actin and 6.43S for 3W-actin. Self-association or dissociation of actin subunits from the complexes was not

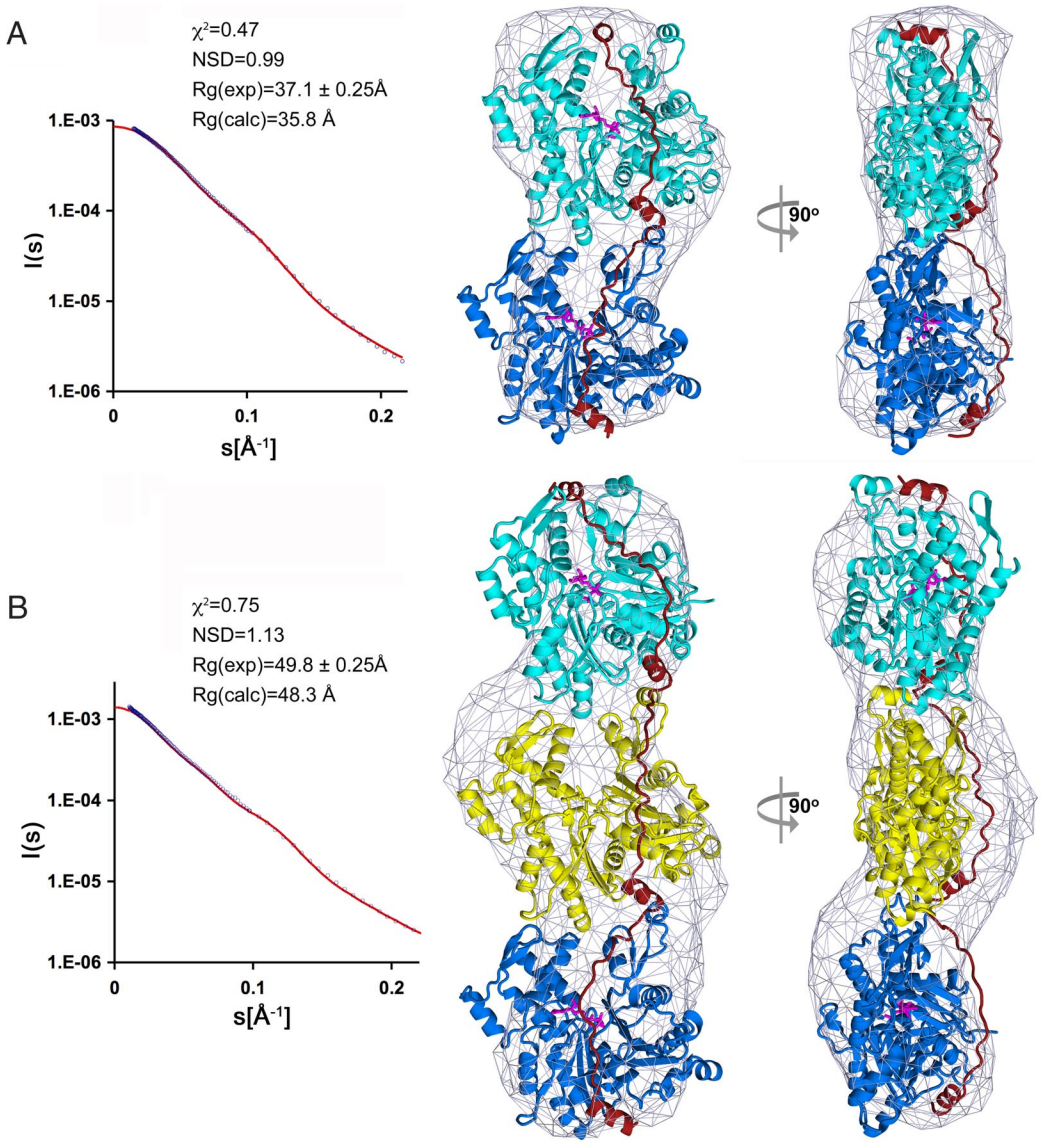

Fig. 2. X-ray scattering models of 2W-actin and 3W-actin. (*A* and *B*) Fitting statistics of the models of 2W-actin and 3W-actin to the scattering data and calculated and experimental R_g values. The data extends to the resolution of ≈28 Å. Two orientations of the models, rotated by 90° and docked into the *ab initio* SAXS envelopes, are shown. Color scheme: actin is blue, yellow, and cyan; W hybrid constructs are red.

observed in sedimentation velocity experiments, even in the presence of phalloidin (a toxin that stabilizes the actin filament) or latrunculin (Fig. 1*E*). The molecular masses of 2W-actin and 3W-actin determined by multiangle light scattering (MALS) coupled with particle separation by field flow fractionation (FFF-MALS) were 90,000 and 125,000 Da (Fig. 1*F*). These values suggested that 2W and 3W form stable complexes with two- and three-actin molecules, with expected masses of 92,038 and 137,161 Da. Therefore, cross-linking of the first W domain to actin Cys-374 and the addition of the C-terminal half of Tβ4 cap the barbed and pointed ends of polymerization nuclei formed by tandem W domains, resulting in monodisperse species suitable for structural investigation.

Study of the Structures of 2W-Actin and 3W-Actin by X-Ray Scattering. To investigate the three-dimensional arrangement of actin subunits in the complexes of 2W-actin and 3W-actin we used x-ray scattering. Similar to electron microscopy (EM), x-ray scattering yields information about the overall shape of macromolecules (15). Some unique advantages of x-ray scattering are that it can be carried out in solution, near physiological conditions, and that it can be applied to smaller molecules than are accessible by single-particle EM. Two overlapping SAXS datasets were collected from each complex at the Biophysics Collaborative Access Team (BioCAT) undulator beamline 18-ID [Advanced Photon Source (APS), Argonne National Laboratory], by using two different sample–detector distances. The merged datasets extended to the resolution of 28 Å (Fig. 2 *A* and *B*). The radii of gyration (R_g), characterizing the overall spread of the particles in solution, were determined from the scattering data with the program GNOM (16), resulting in 37.1 ± 0.25 Å for 2W-actin and 49.8 ± 0.25 Å for 3W-actin. These values suggested that 2W-actin and 3W-actin formed extended complexes in solution.

The solution shapes of 2W-actin and 3W-actin were first reconstructed from the scattering data *ab initio*, by simulated annealing minimization of randomly distributed dummy atom models with the program DAMMIN (17). For each complex, the final envelope consisted of the average, calculated with the

program DAMAVER (18), of 15 *ab initio* dummy atom models. The averaged envelopes had the extended shape characteristic of the long-pitch helix of the actin filament (Fig. 2). Based on this observation, we built atomic models of 2W-actin and 3W-actin (Fig. 1*B*) by superimposing the crystal structure of W-actin onto two or three consecutive subunits of the long-pitch helix of the actin filament (11). To obtain the location of the pointed end capping helix of Tβ4, the structure of actin with the C-terminal portion of Tβ4 (10) was superimposed onto the actin subunit located at the pointed end of each of the complexes. The short and flexible linkers between W domains, which were not visualized in the crystal structures (9), were built *ab initio*. The DNase I-binding loop (or D-loop), corresponding to amino acids His-40–Lys-50 of actin, was modeled according to the structure of monomeric ADP-actin where it is folded as a helix (19). The D-loop is flexible, and among the few structures where it has been observed, the helical conformation was the only one sterically compatible with the binding of the W domain (discussed below).

The resulting atomic models of 2W-actin and 3W-actin fit very well into the *ab initio* SAXS envelopes, as reflected by normalized spatial discrepancy (NSD) values of 0.99 and 1.13, respectively (Fig. 2). The theoretical R_g values calculated from the models of 2W-actin (35.8 Å) and 3W-actin (48.3 Å) are also in good agreement with the experimental values listed above. Furthermore, the theoretical scattering curves calculated from the models by using the program CRYSOL (20) are in excellent agreement with the experimental curves, with discrepancy values, χ^2, of 0.47 and 0.75 for 2W-actin and 3W-actin. Importantly, χ^2 is a more reliable indicator of the agreement of a model with the scattering data than the fit to the *ab initio* envelope (15). These results strongly suggest that the actin subunits in the complexes of 2W-actin and 3W-actin adopt an extended conformation that resembles that of the long-pitch helix of the actin filament.

Discussion

Tandem W domains constitute a common architecture among actin filament nucleators, including Spire (3), Cobl (4), VopL (5), and VopF (6). The isolated W repeats of these proteins account for most of the polymerization inducing activity of the full-length proteins, suggesting that they constitute independent functional modules. Tandem W domains are thought to promote filament nucleation by stabilizing actin subunits into a filament-like polymerization nucleus. Yet, direct visualization of the structure of a primary nucleus had not been achieved, mainly because these complexes represent transient species that evolve rapidly into filaments. We have established a way to stabilize polymerization nuclei by using tandem W domain hybrid constructs that cap the barbed and pointed ends (Fig. 1). Because the design of these constructs is based entirely on high-resolution structures of W-actin (9) and Tβ4-actin (10), this strategy allowed us to visualize actin assemblies formed at the onset of nucleation with minimal structural distortion.

Constructs 2W and 3W form stable complexes with two- and three-actin subunits, respectively (Fig. 1 *C–F*). Analysis of the complexes by x-ray scattering suggests that Spire-like tandem W domains promote polymerization by aligning actin subunits along the long-pitch helix of the actin filament (Figs. 2 and 3). Because the pair of W domains used in constructs 2W and 3W occurs naturally in N-WASP, which is an activator of Arp2/3 complex (2), another conclusion of this work is that N-WASP contributes a long-pitch actin dimer during filament nucleation by Arp2/3 complex. According to a recent study (21), this dimer is added at the barbed end of the actin-related subunit Arp2 of Arp2/3 complex, to form a long-pitch trimer similar to that shown in Fig. 2*B*, consisting of Arp2 and two actin subunits.

The observation that the complexes of 2W-actin and 3W-actin adopt a filament-like conformation suggests that intersubunit contacts along the long pitch helix of the actin filament coexist with the binding of the W domain. The exact nature of intersubunit contacts in the filament is unknown, and it has been proposed that the filament may exist in dynamic equilibrium between multiple states (22). The crystal structure of a cross-linked long-pitch dimer (23) reveals contacts between subdomains 4 and 3 of neighboring actin subunits that are believed to resemble those in the filament. Other long-pitch contacts are thought to involve the D-loop of one actin subunit and the hydrophobic cleft between subdomains 1 and 3 of the next subunit (11–13). The D-loop has rarely been observed in crystal structures of actin. In the fiber diffraction model of the filament

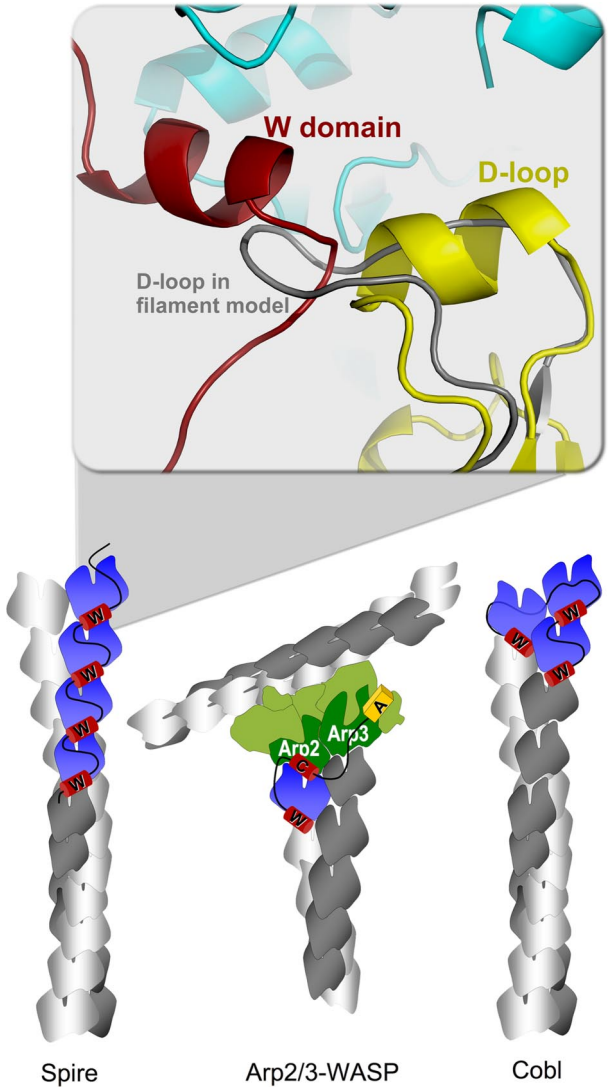

Fig. 3. Model of filament nucleation by W-containing proteins. The nucleation activities of W-based filament nucleators differ widely. A higher nucleation activity in Cobl appears to correlate with a longer linker between the last two W domains (Fig. 1*A*), which is thought to allow this protein to stabilize a short-pitch actin trimer (4). As shown here (see Fig. 2), the shorter linkers of N-WASP and Spire can only connect actin subunits of the long-pitch helix, which may explain the weaker nucleation activity of Spire (3). The linker between the W and C domains of WASP family proteins is also short and may serve to position the first actin subunit at the barbed end of Arp2 during Arp2/3 complex activation (21). (*Inset*) Binding of the W domain between actin subdomains 1 and 3 is incompatible with the conformation of the D-loop (gray) in the filament model (11). To avoid steric clashes, we modeled this loop as a helix (yellow), according to the structure of ADP-bound TMR-actin (19).

(11), the D-loop was modeled as a β-hairpin, corresponding to its conformation in the actin–DNase I complex. Because of steric hindrance, this conformation is incompatible with the binding of the W domain (Fig. 3), which also binds in the hydrophobic cleft in actin (9). Various actin-binding proteins present helices that, like the W domain, bind in hydrophobic cleft in actin, leading us to propose that the D-loop might also assume a helical conformation in the filament (13), corresponding to the conformation of the loop in the structure of ADP-bound TMR-actin (19). We tested here the few structures where the D-loop has been observed crystallographically and found that the helical conformation of the D-loop in TMR-actin is indeed the only one sterically compatible with the binding of the W domain (Fig. 3). However, the D-loop cannot be visualized at the resolution of this work, and it is possible that its conformation in the filament is unlike any of the existing structures of the actin monomer.

There are significant differences in the nucleation activities of W-based nucleators. Thus, the nucleation activity of Spire, which contains four W domains, is relatively weak (3). In contrast, Cobl (4), VopL (5), and VopF (6), with only three W domains, have nucleation activities comparable with that of Arp2/3 complex. Analysis of the sequences (Fig. 1*A*) and three-dimensional arrangement of actin subunits in the complexes of 2W-actin and 3W-actin (Fig. 2) offers important clues concerning the reasons for such differences. Although the W domains of filament nucleators are generally well conserved, significant differences occur in the linkers between W domains and in particular in the linker between the second and third W domains. These differences are crucial because they probably determine the relative arrangement of actin subunits in the polymerization nucleus and thereby the nucleation activities of each protein. When the linkers are short, as in N-WASP and Spire, only actin subunits along the long-pitch helix of the actin filament can be connected (Fig. 3). In Cobl, however, the second linker is significantly longer than in Spire. This longer linker is rich in Pro residues and replaces the third W domain of Spire that, interestingly, differs from canonical W domains in that it also contains a number of Pro residues (Fig. 1*A*). Shortening the second linker reduces dramatically the nucleation activity of Cobl (4). Because a longer linker may allow successive W domains to connect actin subunits on opposite filament strands, this observation led to the proposal that the third actin subunit of the polymerization nucleus of Cobl is positioned laterally with respect to the first two (4) (Fig. 3). If this proposal is correct, a compact nucleus consisting of three actin subunits organized as in the short-pitch filament helix (11) is a more effective way to promote actin polymerization than the Spire nucleus of four actin subunits along the long-pitch helix. In VopL and VopF, the second linker is also rich in Pro residues and longer than any of the linkers of Spire. Because VopL and VopF are strong nucleators, it is tempting to propose that like Cobl these two proteins stabilize a polymerization nucleus consisting of three actin subunits of the short-pitch helix. However, the second linker of VopL and VopF is significantly shorter than that of Cobl (Fig. 1*A*), and because the length of the linker is so critical for Cobl activity (4), the reasons for the strong nucleation activities of VopL and VopF remain a mystery.

Despite intensive investigation, a model of the actin filament obtained from fiber diffraction 18 years ago (11) remains, to this day, the most complete description of intersubunit contacts in the filament. Although a structure of a cross-linked long-pitch dimer is thought to reveal a more accurate picture of contacts involving subdomains 4 and 3 of neighboring subunits (23), this structure lacked the normal twist of the filament, and contacts involving subdomain 2 were not visualized. Even less is known about lateral contacts in the filament, although the role of the hydrophobic loop in this interaction is well documented (for review, see ref. 22). Stabilization of actin filaments for structural studies has been attempted by combining the pointed end-binding protein tropomodulin and a hybrid construct of gelsolin with troponin T (24). Although this approach narrowed the length distribution of actin filaments, a single particle could not be obtained. Hybrid constructs based on tandem W domains offer a unique opportunity to solve this long-standing problem of structural biology. The W domain is the smallest actin-binding motif known, and its actin-bound structure is well characterized (9, 10). As demonstrated by this work, the natural occurrence of tandem W domains linking actin subunits both along and across filament strands offers a unique opportunity to stabilize filament-like actin nuclei for structural studies.

Materials and Methods

Cloning and Expression of Tandem W Hybrid Constructs. The cDNAs of mouse N-WASP and Tβ4 were purchased from American Type Culture Collection. To generate construct 2W, fragments encoding N-WASP residues Ala-397–Lys-444 and Tβ4 residues Lys-20–Ser-44 were amplified by PCR. A 4-bp sequence, corresponding to the 3′-end of the N-WASP fragment, was added at the 5′-end of the Tβ4 fragment for hybridization with T4 DNA polymerase (25). The product was amplified by PCR with a forward primer containing the P398C mutation. N-WASP residue Cys-427 was mutated to Ala by using the QuikChange kit (Stratagene). Construct 3W was obtained by hybridization of two overlapping fragments of construct 2W: Ala-397–Lys-444 and Glu-419 to the C terminus (Fig. 1*A*). To fuse the two fragments, SacI restriction sites were introduced as silent mutations at the 3′-end of the first fragment and the 5′-end of the second fragment. Constructs 2W and 3W were cloned between the SapI and PstI sites of vector pTYB11 (New England BioLabs), containing a chitin-binding domain for affinity purification and an intein for self-cleavage after purification. Both constructs were expressed in BL21(DE3) cells (Invitrogen). Cells were grown in Terrific Broth medium at 37°C until the A_{600} was 1.0–1.2. Expression was induced with 0.5 mM isopropylthio-β-D-galactoside for 5 h at 20°C. Cells were resuspended in chitin-column equilibration buffer [20 mM Hepes (pH 7.5), 500 mM NaCl, 1 mM EDTA, and 100 μM PMSF]. After purification on the chitin affinity column, the proteins were additionally purified on a reverse-phase C18 column (0.1% trifluoroacetic acid and 0–90% acetonitrile). Pure proteins were dialyzed against 2 mM Tris (pH 7.5), 0.2 mM $CaCl_2$.

Formation of the 2W-Actin and 3W-Actin Cross-Linked Complexes. Constructs 2W and 3W were activated with 5,5′-dithiobis(2-nitrobenzoic acid) (DTNB) to facilitate cross-linking to actin Cys-374. The concentration of labeled 2W and 3W was determined by using the extinction coefficient of DTNB at 412 nm (1.36×10^4 M^{-1} cm^{-1}). Actin was purified from rabbit skeletal muscle (26). Activated 2W and 3W were mixed with actin at 1:2.2 and 1:3.2 molar ratios, respectively. Excess actin was removed by gel filtration on a S100 column (Pfizer–Amersham Pharmacia) in 2 mM Tris·HCl (pH 7.5), 100 mM NaCl, 0.2 mM $CaCl_2$, and 0.2 mM ATP. Protein concentration was determined by using theoretical extinction coefficients at 280 nm: 92,430 M^{-1} cm^{-1} for 2W-actin and 138,645 M^{-1} cm^{-1} for 3W-actin.

Analytical Ultracentrifugation. Sedimentation velocity experiments were conducted in a Beckman Optima XL-I ultracentrifuge (Beckman, Palo Alto, CA), by using either an An60 Ti four-hole rotor or an An50 Ti eight-hole rotor. Data were acquired with the interference optics system by using sapphire windows and meniscus-matching 12-mm aluminum-filled Epon centerpieces with interference slit-window holders on the top window (Biomolecular Interaction Technology Center). The 2W-actin and 3W-actin complexes were dialyzed against 2 mM Tris·HCl (pH 7.5), 100 mM NaCl, 0.2 mM $CaCl_2$, and 0.2 mM ATP. Velocity experiments were conducted at 166,000 $\times$ *g* and 20°C. Phalloidin and latrunculin B (both from Sigma) were used in some of the runs. Sedimentation velocity data were analyzed by using the program SEDANAL (27). The S values were converted to standard $S_{20,W}$ values (sedimentation coefficient at 20°C in water) with the program SEDNTERP (28).

FFF-MALS. The masses and monodispersity of 2W-actin and 3W-actin were analyzed by using an Eclipse asymmetric FFF system coupled with a DAWN HELEOS MALS detector and an Optilab rEX refractometer (Wyatt Technology). This configuration allows for the determination of the molar masses of the species separated by the FFF unit. The FFF channel was fit with a 350-μm Teflon spacer over a 10-kDa cutoff cellulose membrane. One hundred microliters of each sample (1 mg/ml) was injected by using an HPLC system, which also delivered the mobile phase for the FFF unit. Samples were first focused for 6 min at the head of the channel by using two opposite lateral flows of 1 ml/min and a vertical cross-flow of 2 ml/min and then eluted with a single lateral flow

of 1.0 ml/min and a cross-flow of 2 ml/min. Samples eluting in order of increasing size were detected by the refractometer and the 18-angle MALS detector (equipped with a 50-mV solid-state laser operating at 658 nm). Baseline scattering, peak boundaries, and molecular masses were determined by using the Astra software (Wyatt Technology).

SAXS Data Collection and Analysis. SAXS datasets were collected from solutions of 2W-actin and 3W-actin at the BioCAT undulator beamline 18-ID of the APS, Argonne National Laboratory (29). To minimize radiation damage during data collection, samples were continuously pumped through a 1.5-mm-wide quartz capillary at 12.5 μl/s for an average exposure time of 0.6s. Two SAXS datasets were collected from each complex at the sample–detector distances of 2,804-mm and 180 mm. The measurements were performed at 10°C and at two different concentrations per sample and per camera length. Thus, 2W-actin was collected at 0.25 and 2 mg/ml (long camera length) and 2 and 8 mg/ml (short camera length). Similarly, 3W-actin was collected at 0.25 and 0.5 mg/ml (long camera length) and 4.5 and 9 mg/ml (short camera length). Concentration-dependent systematic differences were not observed, indicating the absence of interparticle interference. Protein scattering profiles were obtained by subtracting the average of 20 buffer-only profiles from the average of 20 protein-buffer profiles. The overlapping scattering profiles corresponding to the two camera-lengths were merged in the s range 0.005 to 0.25 Å^{-1} with the program IGOR Pro (WaveMetrics), and macros written by the BioCAT staff. The R_g and maximum particle dimensions, D_{max}, were computed with the indirect transform package GNOM (16), which also gives the distance distribution functions $p(r)$. *Ab initio* shape reconstructions were performed with the program DAMMIN (17), which represents a macromolecule as an assembly of densely packed beads. This program uses simulated annealing to build a compact interconnected configuration of beads inside a sphere with diameter D_{max} that fits the experimental data $I_{exp}(s)$ to minimize discrepancy:

$$\chi^2 = \frac{1}{N-1}\sum_j \left[\frac{I_{\exp}(s_j) - cI_{\text{calc}}(s_j)}{\sigma(s_j)}\right]^2, \qquad [1]$$

where N is the number of experimental points, c is a scaling factor and $I_{calc}(s_j)$ and $\sigma(s_j)$ are the calculated intensity and experimental error at the momentum transfer, s_j. For each of the complexes, 15 *ab initio* models were generated and averaged by using the program DAMAVER (18). Atomic models were fit into the *ab initio* envelopes with the program SUPCOMB (30). This program minimizes the NSD, which is the normalized average of the distances between every point s_{1i} of structure 1 and all points s_{2i} of structure 2 [$\rho(s_{1i},2)$], and every point s_{2i} of structure 2 and all points s_{1i} of structure 1 [$\rho(s_{2i},1)$]:

$$\text{NSD}(1,2) = \left[\frac{1}{2}\left(\frac{1}{N_1 d_2^2}\sum_i^{N_1}\rho^2(s_{1i},2) + \frac{1}{N_2 d_1^2}\sum_i^{N_2}\rho^2(s_{2i},1)\right)\right]^{1/2}, \qquad [2]$$

where N_1 is the number of points (atoms or dummy atoms) and d_1 is the average distance between adjacent points in a structure. The theoretical scattering curves from the atomic models were calculated and compared with the experimental curves with the program CRYSOL (20).

ACKNOWLEDGMENTS. This work was supported by National Institutes of Health Grant HL086655. Synchrotron data collection was supported by Department of Energy Contract W-31-109-ENG-38 (to APS) and National Institutes of Health Grant RR08630 (to BioCAT).

1. Sept D, McCammon JA (2001) Thermodynamics and kinetics of actin filament nucleation. *Biophys J* 81:667–674.
2. Pollard TD (2007) Regulation of actin filament assembly by Arp2/3 complex and formins. *Annu Rev Biophys Biomol Struct* 36:451–477.
3. Quinlan ME, Heuser JE, Kerkhoff E, Mullins RD (2005) *Drosophila* Spire is an actin nucleation factor. *Nature* 433:382–388.
4. Ahuja R, *et al*. (2007) Cordon-bleu is an actin nucleation factor and controls neuronal morphology. *Cell* 131:337–350.
5. Liverman AD, *et al*. (2007) Arp2/3-independent assembly of actin by *Vibrio* type III effector VopL. *Proc Natl Acad Sci USA* 104:17117–17122.
6. Tam VC, Serruto D, Dziejman M, Brieher W, Mekalanos JJ (2007) A type III secretion system in *Vibrio cholerae* translocates a Formin/Spire hybrid-like actin nucleator to promote intestinal colonization. *Cell Host Microbe* 1:95–107.
7. Chereau D, *et al*. (2008) Leiomodin is an actin filament nucleator in muscle cells. *Science* 320:239–243.
8. Dominguez R (2007) The β-thymosin/WH2-fold: Multifunctionality and structure. *Ann NY Acad Sci* 1112:86–94.
9. Chereau D, *et al*. (2005) Actin-bound structures of Wiskott–Aldrich syndrome protein (WASP) homology domain 2 and the implications for filament assembly. *Proc Natl Acad Sci USA* 102:16644–16649.
10. Irobi E, *et al*. (2004) Structural basis of actin sequestration by thymosin-β4: Implications for WH2 proteins. *EMBO J* 23:3599–3608.
11. Holmes KC, Popp D, Gebhard W, Kabsch W (1990) Atomic model of the actin filament. *Nature* 347:44–49.
12. Hegyi G, *et al*. (1998) Intrastrand cross-linked actin between Gln-41 and Cys-374. I. Mapping of sites cross-linked in F-actin by *N*-(4-azido-2-nitrophenyl) putrescine. *Biochemistry* 37:17784–17792.
13. Dominguez R (2004) Actin-binding proteins: A unifying hypothesis. *Trends Biochem Sci* 29:572–578.
14. Coue M, Brenner SL, Spector I, Korn ED (1987) Inhibition of actin polymerization by latrunculin A. *FEBS Lett* 213:316–318.
15. Petoukhov MV, Svergun DI (2007) Analysis of x-ray and neutron scattering from biomacromolecular solutions. *Curr Opin Struct Biol* 17:562–571.
16. Svergun DI (1992) Determination of the regularization parameter in indirect-transform methods using perceptual criteria. *J Appl Crystallogr* 25:495–503.
17. Svergun DI (1999) Restoring low-resolution structure of biological macromolecules from solution scattering using simulated annealing. *Biophys J* 76:2879–2886.
18. Volkov VV, Svergun DI (2003) Uniqueness of *ab initio* shape determination in small-angle scattering. *J Appl Crystallog* 36:860–864.
19. Otterbein LR, Graceffa P, Dominguez R (2001) The crystal structure of uncomplexed actin in the ADP state. *Science* 293:708–711.
20. Svergun DI, Barberato C, Koch MH (1995) CRYSOL: A program to evaluate x-ray solution scattering of biological macromolecules from atomic coordinates. *J Appl Crystallog* 28:768–773.
21. Boczkowska M, *et al*. (2008) X-ray scattering study of activated Arp2/3 complex with bound actin-WCA. *Structure* 16:695–704.
22. Reisler E, Egelman EH (2007) Actin structure and function: What we still do not understand. *J Biol Chem* 282:36133–36137.
23. Kudryashov DS, *et al*. (2005) The crystal structure of a cross-linked actin dimer suggests a detailed molecular interface in F-actin. *Proc Natl Acad Sci USA* 102:13105–13110.
24. Gong H, *et al*. (2005) Mini-thin filaments regulated by troponin-tropomyosin. *Proc Natl Acad Sci USA* 102:656–661.
25. Aslanidis C, de Jong PJ (1990) Ligation-independent cloning of PCR products (LIC-PCR). *Nucleic Acids Res* 18:6069–6074.
26. Pardee JD, Spudich JA (1982) Purification of muscle actin. *Methods Enzymol* 85:164–181.
27. Stafford WF, Sherwood PJ (2004) Analysis of heterologous interacting systems by sedimentation velocity: Curve fitting algorithms for estimation of sedimentation coefficients, equilibrium and kinetic constants. *Biophys Chem* 108:231–243.
28. Laue TM, Shah BD, Ridgeway TM, Pelletier SL (1992) *Analytical Ultracentrifugation in Biochemistry and Polymer Sciences*, eds Harding SE, Rowe AJ, Horton JC (Royal Society of Chemistry, Cambridge, UK), pp 90–125.
29. Fischetti R, *et al*. (2004) The BioCAT undulator beamline 18ID: a facility for biological noncrystalline diffraction and X-ray absorption spectroscopy at the Advanced Photon Source. *J Synchrotron Radiat* 11:399–405.
30. Kosik KS, Svergun DI (2001) Automated matching of high- and low-resolution structural models. *J Appl Crystallog* 34:33–41.